Journal of
Marine Science and Engineering

MDPI

Article

Techno-Economic Analysis of Axial-Flow Current Turbines Applied to the US Virgin Islands

Jonisha Aubain * and Erin Baker

Department of Mechanical and Industrial Engineering, University of Massachusetts Amherst, Amherst, MA 01003, USA; edbaker@umass.edu
* Correspondence: jaubainbeix@umass.edu

Abstract

The Small Island Developing States (SIDS) face a myriad of energy challenges due to their dependence on imported fossil fuels and increased rates of natural disasters, resulting in high electricity costs and grid instability. Marine current energy continues to be an emerging energy technology because of high installation and maintenance costs; however, the large resource availability makes it a promising resource for islands. This study is a techno-economic evaluation of a novel bridge-supported marine current energy system designed for shallow-water deployment, using the U.S. Virgin Islands as a case study. A bridge support structure is proposed that will allow for ease of installation and maintenance within local systems. The National Renewable Energy Laboratory (NREL) Reference Model 4 was used as the framework for the technical design and cost estimates and was adjusted based on economies-of-scale relationships. We develop an estimate for the levelized cost of energy (LCOE) for installations for a range of deployments and perform sensitivity analysis over current velocity correction factors, turbine size, and interest rate. The results indicate that a three-unit installation for this case study will achieve an LCOE of \$1.13/kWh, while 100-unit deployments can reduce the LCOE to \$0.31/kWh. The technology becomes economically competitive with the present electricity cost in the U.S. Virgin Islands—\$0.42/kWh—at an installed capacity of approximately 10 MW. These findings demonstrate the potential of bridge-supported marine current energy systems to strengthen energy security and support the renewable energy transition in the Caribbean and other Small Island Developing States.

Keywords: renewable energy; marine energy; levelized cost of energy; Caribbean energy development; SIDS

Check for updates

Academic Editors: Constantine Michailides and Alberto Peña

Received: 21 August 2026
Revised: 10 September 2026
Accepted: 12 September 2026
Published: 16 September 2026

1. Introduction

Energy has long been a challenging issue for island nations. The need for importing oil and gas for traditional generating units has led to expensive and often unreliable electrical systems. However, when looking at alternative energy sources, conventional renewable energy technologies are often incompatible with island conditions. The land area for solar power is often scarce; wind resources can be relatively low, especially for islands in tropical and subtropical regions; and the limited freshwater availability, compounded by droughts [1], along with the flat terrain of some regions can make hydropower difficult to apply. However, island nations are surrounded by oceans, presenting a promising energy resource. According to IRENA, the global resource potential from ocean and tidal currents ranges between 20,000 TWh and 80,000 TWh of electricity per year [2]. Axial-flow current turbines, also known as tidal turbines, convert the kinetic energy of moving water into electrical power and are typically deployed in locations with strong, predictable currents [3].

At the same time, the energy systems of small island states face a myriad of challenges, including structural vulnerabilities, high import dependence, and limited adaptability to economic disruptions and natural disasters. Small Island Developing States (SIDS) are a group of 39 states and 18 associating members that have similar economic and environmental challenges related to their geographical location and long-standing colonial impacts [4]; 90% of the SIDS's energy generation comes from imported petroleum, compared to the global average of 21% [5,6]. This heavy fossil fuel dependence exposes the islands to price volatility and potential supply disruptions. The aging infrastructure and the long-term impacts of natural disasters further exacerbate the vulnerability of these locations due to unreliable electrical networks and high restoration costs [7–11]. Financial constraints limit the ability to modernize grids or invest in large-scale energy transition. Thus, identifying resilient and locally available energy resources remains a priority.

Resource assessments for installed marine energy projects have identified high average current speeds and water depths greater than 25 m as key criteria for site viability [12–14]. However, the SIDS are often characterized by moderate current speeds and shallower bathymetry—conditions that can reduce the feasibility of traditional marine energy systems, particularly fixed-bottom or floating tidal technologies [15,16]. In addition, these technologies often require specialized vessels and infrastructure for installation due to their size and weight, making local fabrication unlikely. This reliance on imported expertise and equipment may extend throughout the project life-cycle, including operation and maintenance (O&M) requirements.

On the other hand, archipelagic topography often creates narrow channels between islands that accelerate local currents. Case studies examining channel utilization worldwide have shown that tidal projects installed in narrow channels have a higher overall power coefficient than tidal projects in the open ocean [17–20]. These geographic features create an opportunity to re-examine system design for island environments.

Although tidal energy can offer predictable generation profiles, high upfront capital expenditures (CAPEX) and significant operating and maintenance expenditures (OPEX) have led to limited installed capacity. The OPEX of marine energy is the highest among variable renewable energy technologies and often contributes to project failure due to higher-than-expected costs and project underperformance [21].

Most levelized cost of energy (LCOE) analyses for tidal systems focus on traditional fixed seabed-mounted or floating platforms, which have high costs due to the need for specialized vessels and offshore installation. These studies have highlighted the need for more comprehensive cost data to improve the economic projections for the growth of this technology [22–24]. Alternative structural approaches that can reduce the complexity and cost of project development, particularly in the environmental conditions typical for the SIDS, are limited in the present research.

This study presents a preliminary design and economic analysis of a bridge-supported structure to accommodate an array of turbines, specifically targeting site conditions observed for our case study in the US Virgin Islands. The proposed configuration is a bridge structure that supports 29 turbines, positioned within shallow inter-island channels. By elevating the support structure above sea level, the design improves accessibility for installation and maintenance while reducing dependence on offshore vessels. This design also allows turbine placement near the sea surface, allowing operation in higher-velocity flow regions and increasing energy extraction potential [25,26].

This design is applied to channel conditions in the US Virgin Islands, using bathymetry and current velocity data. This system is intended to be a scalable framework, adaptable to other islands and coastal locations with similar characteristics, including shallow depths and moderate current speeds. The primary objective of this paper is to evaluate the technical feasibility and economic performance of the proposed bridge-supported tidal configuration for SIDS applications. This is done by estimating the LCOE while varying deployment scales, ranging from single-unit to 100-unit installations.

The rest of this paper is organized as follows: Section 2 describes the case study location. Section 3 describes the technical design of our model and the bridge support structure. Section 4 outlines the capital and operating cost estimates that are used to estimate the LCOE. In Section 5, we summarize the LCOE results, and Section 6 discusses challenges and implications for scaling and broader adoption in island contexts.

2. Case Study: US Virgin Islands

The US Virgin Islands (USVI) was selected for this case study due to having an energy landscape typical of the SIDS, as well as the availability of resource data. The USVI has one of the highest electricity costs in the country, rivaling the residential costs of Hawaii, at $0.40–$0.42/kWh, and with commercial costs reaching as high as $0.47/kWh [27,28]. These costs are heavily dependent on the cost of imported fossil fuels, including diesel and liquefied petroleum gas (LPG), which account for 47% and 51% of the energy consumption, respectively, for the territory [29]. Consistent natural disaster impacts, along with aging infrastructure and increased load, contribute to frequent power outages and system failure across the territory [30,31].

The topography of the US Virgin Islands contains many natural channel formations that can produce elevated current speeds and power densities relative to the surrounding open ocean. These flow-constrained locations make promising sites for current energy extraction. Examples of case studies on tidal streams include Pentland Firth and the Alderney Race in Europe, where current speeds have been recorded to reach over 3 m/s [32,33]. The NREL's model reference deployment site was the Gulf Stream off the southeast coast of Florida, due to its high current potential and average depth of 120 m [34].

In contrast, our site has an average depth of 6–8 m and more moderate current speeds. We chose three channels in the US Virgin Islands across the St. Thomas/St. John district. Figure 1 shows a satellite image of St. Thomas, with subfigures of the three channels that we analyzed. These sites were selected because the channels exhibit similar dimensions of approximately 150 m in length and have average current speeds of 1.4 m/s, indicating the potential for acceptable power output. Site 1 is located on the west side of St. Thomas, with the channel extending to a small land mass called West Cay. Sites 2 and 3 are located on the southeast side of the island, with the channels extending from St. Thomas to an island known as Great Saint James; the two channels are separated by another land mass known as Current Rock. The three sites have depths varying between 6 and 8 m [35]. Our structure and turbine specifications are identical for each site and will meet the minimum depth of 6 m. Each site will have identical bridge structures that extend from one land mass to the corresponding land mass on the other side of the channel.

The identification of high-velocity sites was informed by local marine users, particularly commercial fishermen who have extensive knowledge of the region's flow conditions. This knowledge, combined with a tidal resource assessment presented by [36], contributed to the identification of the three candidate sites within this study and validated using Ocean Modeling System data. Figure 2 presents one of the main high-opportunity indicators, a map of the tidal steepness parameter from [37], which identifies locations in the upper Caribbean region with high tidal opportunity. The sites with the highest tidal flow are located across the Virgin Islands, with one of the sites being on the southeast side of St. Thomas.

Although these sites have individual qualities, they provide a reasonable initial test case relevant for many of the SIDS. For example, the Bahamas, Fiji, and the Maldives also each have a large cluster of islands like the Virgin Islands, with many natural channel formations that have similar depths and current constraints.

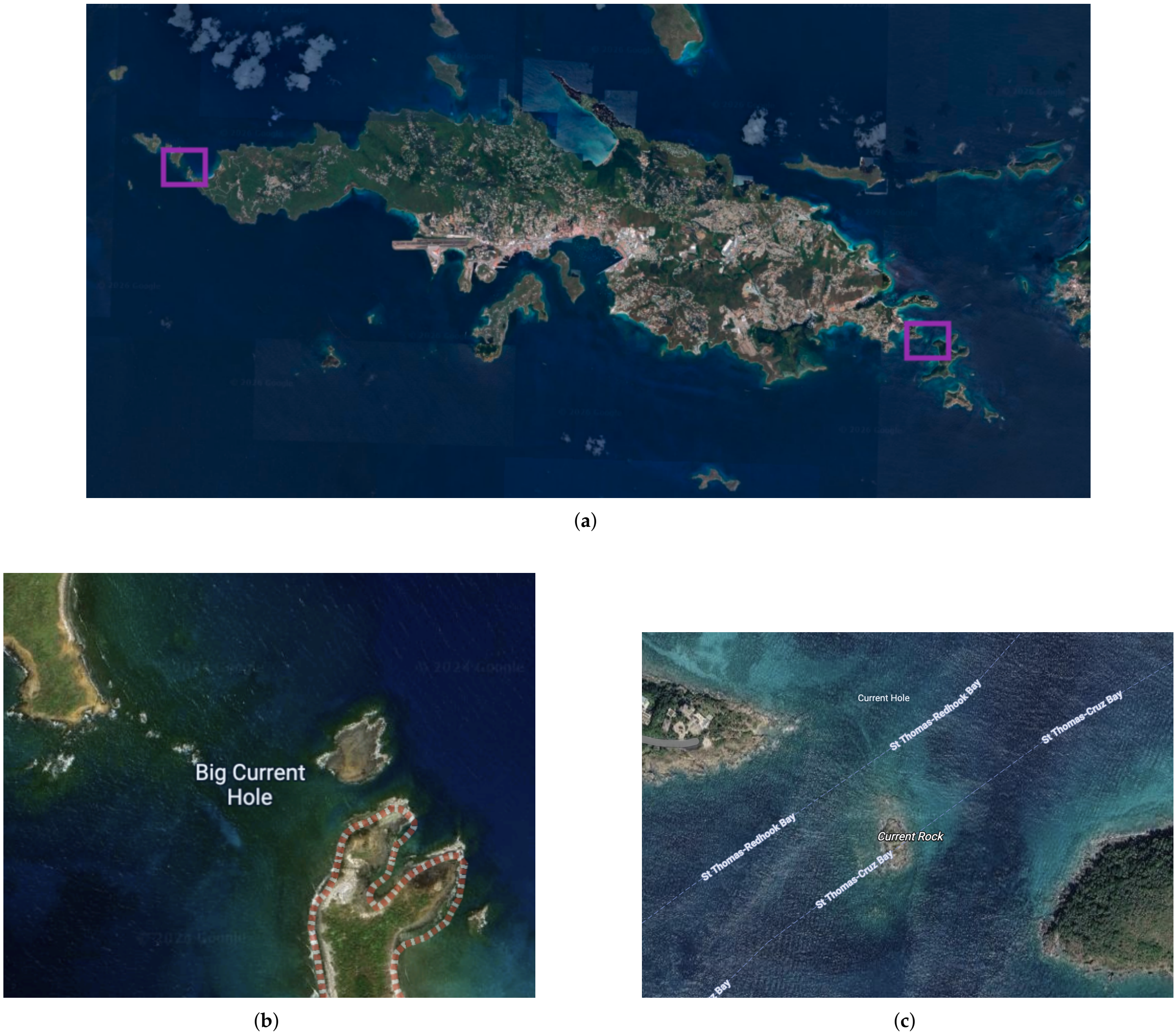

Figure 1. The three channels around St.Thomas and St. John selected for the case study. The purple boxes are the locations of the sites in our case study. (**a**) Map of St. Thomas taken from Google Earth. (**b**) Site 1 is a channel located on the northwest side of St. Thomas and an island called West Cay. Picture taken from Google Maps. (**c**) Sites 2 and 3 are channels located at the southwest side of the island from St. Thomas to Great St. James, with a land mass separating the two sites. Picture taken from Google Maps.

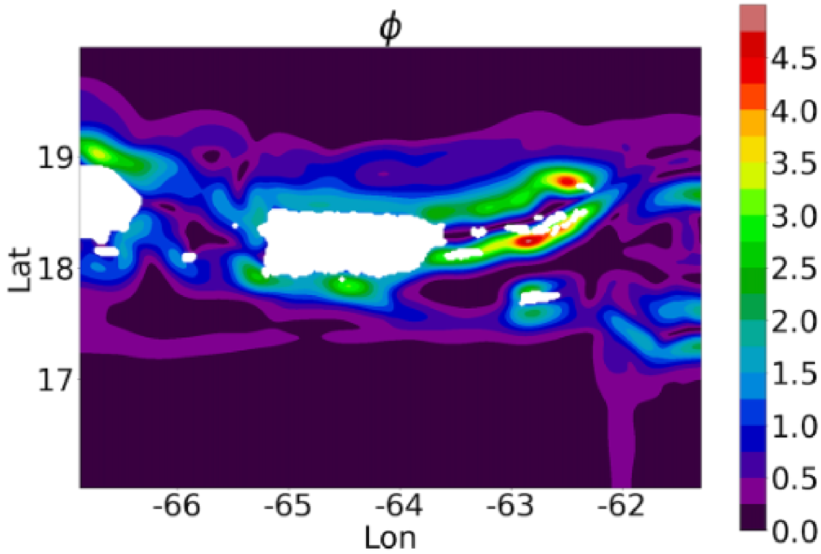

Figure 2. Tidal steepness parameter map taken from the USCROMS model, reproduced from Mukherjee et al. (2023) [37] with permission from Springer Nature in 2025. Note that the large island in the middle is PR; the red areas on the right at latitude 18 represent high tidal opportunities on the southeast side of St Thomas and a small area on the southeast side of St John. The area at latitude 19 is northwest of St. Thomas.

3. Bridge-Supported Marine Energy System Design

In this section, we detail the key aspects of the technical design for the proposed model. We start with a description of the NREL RM4 model and its parameters, followed by an overview of our model and the primary design decisions. We explicitly evaluate the structural feasibility and present the final design parameters used to estimate costs in Section 4.

3.1. Technical Design Methodology

In 2015, the NREL presented a set of reference models for hydrokinetic and marine energy converters [38]. Figure 3 shows the NREL's RM4 marine energy converter. This configuration is designed as a moored floating support structure with four attached turbine rotors and one central rotor-less nacelle to house power electronics. Each rotor has a diameter of 33 m, and the buoyant wing is 120 m long. An in-depth cost analysis was performed for each component of the capital costs (CAPEX) and operating expenditures (OPEX) [39,40].

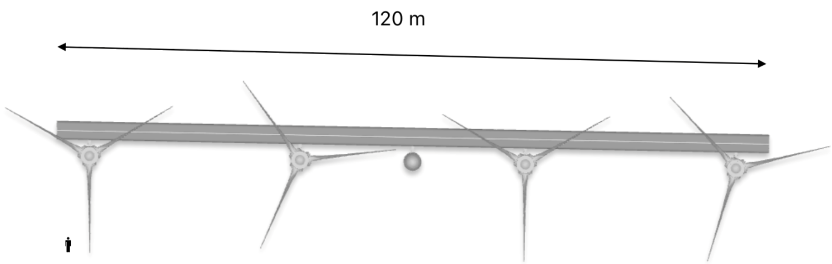

Figure 3. Illustration adapted from the RM4 full-scale geometry. Reproduced with permission from [39], with permission from Sandia National Laboratories, 2026.

One disadvantage of the RM4 configuration is the instability of the floating platform. Moored renewable energy systems are found to drive many hydrodynamic issues that can reduce mechanical efficiency and incur high project costs for installation, operation, and maintenance [41–43]. In addition to this, the turbine size proposed in the NREL model can not be applied to sites shallower than 60 m in depth [44,45]. The largest hydrokinetic tidal project that has been tested or is in phase for further development is a 17 m rotor [46]. Most case studies that analyze larger turbines are theoretical due to technical limitations. This depth requirement and lack of potential manufacturing opportunities make it an unlikely energy option for the SIDS.

To make this more technically applicable for SIDS implementation, we adjusted the design in [47] in the following ways:

1. Reduced the size of the rotor to 3 m in diameter and increased the number of turbines to 29.
2. Introduced a fixed bridge support structure, using a Pratt-truss design.
3. Designed rotors to be suspended from the bridge support structure.

Figure 4 presents an illustration of our Pratt-truss bridge-supported design that is 150 m in length. The number of turbines installed on the bridge was driven by the depth restriction of the three sites [48]. The choice of 29 turbines allows for maximum power output while meeting technical channel system restrictions (i.e., blockage ratio, boundary layer effects, etc.) and the structural loads [49,50]. These changes and their impacts on capacity are detailed in Table 1.

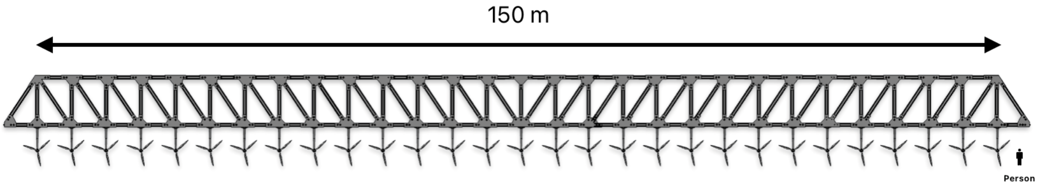

Figure 4. Bridge model with the support structure above sea level and the 29 axial-flow turbines hanging by cylindrical towers from a Pratt-truss bridge structure.

Table 1. Technical specifications for 1 unit.

	NRELs RM4 Model	Bridge Supported Model
Radius	16.5 m	1.5 m
Support Structure Length	120	150
Capacity (per turbine)	1000 kW	8.3 kW
Capacity (per unit)	4000 kW	239.7 kW
Number of Rotors per Unit	4	29

We introduce a fixed Pratt-truss support structure, with the turbines being supported by towers connected to the base of the bridge. This configuration allows for an individual nacelle that houses the power electronics to be stored above sea level, which can facilitate easier operation and maintenance through access to both the rotors and power electronics without special machinery. The tower length was determined based on sea-level rise, maximum wave height recorded by the NOAA, and local tidal variations. The distance between mean sea level and the bridge was selected at 8 m to reduce the effect of direct wave loads on the bridge support structure. We assumed that the rotor has a cut-in speed of 0.8 m/s and cut-out speed of 4 m/s, to replicate the NREL model. This was used to determine annual energy production and thrust loads. More details are provided in Section 3.2, and technical specifications of the bridge are detailed in Table 2. Note that the NREL RM4 model has a symmetric structure and blade profile to operate in bidirectional tidal current flows. As the mechanical components, including the blades and location of the nacelle, are consistent with the original RM4 model, we will assume that the turbines for our model will also operate bidirectionally.

Table 2. Pratt-truss support structure characteristics.

Parameter	Value
Bridge Structure	
Bridge Length	150 m
Bridge Height (from base to top)	8.5 m
Bridge Width	5 m
Beam Length Between Joints	5 m
Number of Members (each side)	117
Number of Members Along Base	29
Maximum Load Before Self-Weight	3138 kN (705 kips)
Maximum Load After Self-Weight	15,427 kN (3468 kips)
W-Section Beam	W14 × 311
Tower Structure	
Tower Length	11 m
Tower Radius	20 cm
Tower Wall Thickness	1 cm
Round HSS Section	HSS 16 × 0.438

3.2. Support Structure

Here, we explain the design choices, calculations, and assumptions made to determine structural feasibility. First, a Pratt-truss bridge was selected because it is stable over longer distances [51,52]. Design decisions were driven by channel length, bridge structural constraints, and hydrodynamic behaviors and specified through an iterative analysis of member lengths and stress distributions. The two main loads considered in this study are axial loads, for the truss structural analysis, and thrust loads, for the tower deflection analysis. The axial loads created by the turbine, the weight of the supporting towers, and the self-weight of the bridge create tension and compression forces on each member, which have different magnitudes throughout the span of the bridge. To determine these forces, we analyzed the truss structure as a 2D model and calculated the corresponding forces for each individual member using the method of joints. Figure 5 shows a 2-dimensional representation of our Pratt bridge with a turbine placed at each joint. This configuration allows for the axial loads of the turbine to be transferred directly through the joint connections, resulting in the ultimate design containing 29 turbines in total. The final bridge truss structure has a total of 264 steel members (i.e., individual connecting beams). Member dimensions were selected to prevent buckling and yield under the maximum loads experienced at the center of the bridge [53]. The maximum force calculated was 3138 kN, given a horizontal beam length of 5 m. According to the American Institute of Steel Construction design specifications, a W14 × 311 I-beam would meet the load of the turbines and the self-weight of the bridge [54].

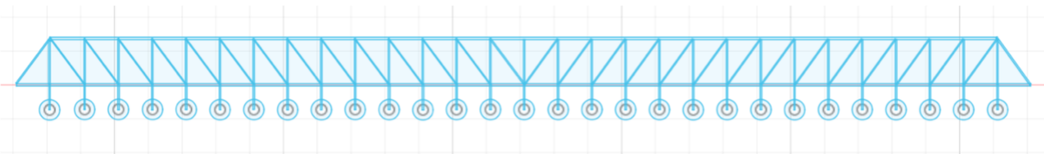

Figure 5. 2D drawing of the Pratt truss bridge concept with 29 turbines hanging from the base of the structure.

We note that although the bending moment created by the thrust force is not explicitly modeled in the truss analysis, we account for it through conservative design assumptions within the thickness of the beams. This thickness was determined through the load calculations and included in the iterative analysis of the members.

The turbine support tower is a cylindrical hollow beam that connects the turbine to the bridge foundation. Each tower is analyzed as a cantilever beam that is fixed at one end (connected to the bridge) and has a point load at the other end (the turbine). The length of the cylinder is estimated above and below sea level. To determine the height of the bridge, we consider the sea-level rise for the next 100 years and the height of extreme waves [35]. Therefore, the length of the cylinder from the bridge to sea level will be 8 m. The tower is 3 m from sea level to rotor hub to account for boundary-layer effects and the possibility of floating debris. With these considerations, the final tower length is 11 m. To determine the beam thickness, we use the maximum deflection equation (Equation (1)) that is used for wind turbine tower deflection analysis [55]:

$$\delta_{max} = \frac{F_T L^3}{3EI} \tag{1}$$

This equation uses the thrust force, F_T; the length of the tower, L; the steel modulus, E; and the moment of inertia, I, which is a function of the tower's inner and outer radius. A Round HSS 16 $\times$ 0.438 was selected to meet the maximum deflection criteria after further iterative analysis. See Table 2 for the dimensions and specifications of the bridge and tower.

We note that our structural study does not consider dynamic loads, including wind and wave loads under extreme storm conditions, or seismic loads. This will be considered in future design optimization work and will be used to validate some of these initial member dimensions.

4. Capital and Operating Cost Estimation Analysis

Cost estimates for our model were derived from the published techno-economic analysis of the RM4 model and informed by related studies to support a robust justification of our assumptions [56,57]. Adjustments to this analysis were made to account for the structural and environmental differences of our proposed model and are presented throughout this section. We note that, for both models, we used the term "unit" to indicate a single structure with the corresponding number of turbines attached; that is, in this case, a unit refers to the bridge with 29 turbines. Other cost estimates for different turbine and farm sizes were taken from [18,58] to develop our estimates and determine plausible ranges for projects of this scale.

4.1. Cost Categories and Methods

CAPEX includes all costs associated with the installation and commissioning of the technology. OPEX includes all costs that recur over the project's lifetime [59]. CAPEX is divided into five categories: The first category, Power Take-Off, encompasses all components within the rotor nacelle assembly. The second category, Installation, includes cable landing, transport, and device installation costs. We note that our support structure eliminates some of the "infrastructural" needs associated with a moored support structure, most particularly the maintenance vessel. The third category, Support Structure, is estimated using the unit cost of steel and the cost of structural development, which is based on the size of the bridge. The fourth category, Development, includes site assessment, permitting, and project management. The fifth category, Contingency, accounts for unknown costs that occur throughout the project development; we set this cost to be 8% of the CAPEX. Finally, OPEX includes annual insurance, shore-side operations, and replacement parts.

We note that the operation and maintenance of any marine energy technology is very complex and continues to be difficult to capture in marine energy studies. While this is the case, our operation and maintenance values are taken from the NREL model and scaled directly for the capacity of our system. The staging and operation site used for the RM4 case study is in the strait between the east coast of Florida and Grand Bahama Island. This means that the environmental and storm conditions under which the NREL model is analyzed are relatively similar to our case study site; thus, we can assume similar operation and maintenance logistics to address it. We note that there are two countervailing effects on the OPEX costs: On the one hand, some of the advantages in our system (above-sea-level nacelle and turbines closer to the surface, accessible from the bridge) are likely to reduce OPEX costs. On the other hand, some of the challenges faced by the SIDS may increase OPEX costs. Thus, other than removing the installation vessel, we have based our cost estimates on the NREL study.

Some key assumptions applied to ensure consistency throughout our model are as follows:

- The power coefficient, which is the ratio of power produced to the resource power potential [60], is assumed to remain constant throughout the lifetime of the system
- Rotors are assumed to rotate with the tidal direction, consistent with the RM4 model

The following subsection, Section 4.2, describes how we estimate the cost of the support structure. Then, Section 4.3 describes how we scale the cost estimates from the RM4 to match our design, considering rotor size, capacity, and mass, as well as farm size. Section 4.4 presents the resulting estimates for the capital and operating costs.

4.2. Support Structure Cost Analysis

The cost of the support structure is made up of two parts: the cost of the steel members, and the structural development. Steel members include the beams of the bridge and the towers that support the turbine. We assume that the cost of the beams is \$1.00/lb/ft, which gives a cost of \$311/ft for each member [61]. Given the total amount of steel throughout the bridge for all 264 members, the cost of the bridge is \$1.75 million. The structural development was based on similarly sized bridges and included the following considerations: labor, equipment, concrete (for foundation at the ends of the bridge), bolts, welds, site preparation, management, and transport of members [62]. A cost range for the structural development of a heavy-duty bridge is \$800–\$1200 per square meter [63,64]. This results in a cost range of \$600,000–\$900,000; we chose the middle estimate of \$750,000 for our analysis. After dividing by the capacity for the 1-unit array of 2.636 MW, our resulting CAPEX cost is \$7300/kW for the steel members and \$3129/kW for the structural development, for a 1-unit array. We assume that the cost per kW of steel will remain the same as the farm size increases. However, the structural development has been shown to reduce as production increases; thus, we apply the farm scaling discussed in the subsection below [65].

4.3. Cost Scaling

Here, we describe the scaling equations that are used to move from the estimates in the NREL literature to our model. Table 3 identifies the type of scaling applied to different elements of the design and is detailed in the following subsections.

4.3.1. Cost Scaling by Turbine Radius

The size of the rotor directly determines the energy capture and the loads incurred from the blades. The concept is that (1) the cost of the turbine blades, not including the rotor nacelle assembly, will increase linearly with turbine radius; and (2) the power generated by a rotor increases with the square of the radius. This implies that the cost per kW will decrease linearly in the radius. Thus, the equation for scaling the cost by the radius is as follows:

$$C_{r1} = C_{r2} * \frac{r_2}{r_1} \tag{2}$$

where C_{r_i} is the cost of a unit with radius r_i. This relationship accounts for reduced material usage and reduced energy capacity in smaller rotors. This scaling is applied to the rotor size. Details of the equation derivation are presented in Appendix A.

Table 3. Scaling breakdown. We note that all components are scaled with the capacity of the installation; thus, we do not put this in the table.

	Elements	Scaling
CAPEX		
Power Take-Off		
	Rotor	Scaled w/Radius
	Nacelle	No scaling [1]
Installation		
	Cable Shore Landing	Scaled with per-unit capacity
	Device Installation	Scaled with mass
	Cabling	No scaling
	Transport to Site	No scaling
Support Structure		
	Amount of Steel	N/A
	Bridge Installation and Fabrication	N/A
Development		
	All Elements	Scaled with per-unit capacity
OPEX		
	All Elements	Scaled with per-unit capacity

[1] Note that all costs are calculated on a per-capacity basis, per kW. Thus, elements that have a fixed cost per kW regardless of the scale, are identified as "no scaling" in the table.

4.3.2. Cost Scaling Per-Unit Capacity

The scaling based on unit capacity is applied to the Development, OPEX, and cable shore landing. We assume that these three items have a cost that is largely fixed and independent of the size of the project. This scaling is applied to the entire unit, rather than the individual turbines. The equation for this scaling is as follows:

$$C_{r1} = C_{r2} * \frac{Q_2}{Q_1} \tag{3}$$

For this equation, Q_i represents the power capacity of unit i, measured in kW. Note that our unit has a capacity of 240 kW and the NREL's model has a unit capacity of 4000 kW. Thus, we will see an increase in the cost per unit of capacity for our estimates.

4.3.3. Cost Scaling by Mass

Device installation costs are assumed to scale with mass. The assumption is that heavier equipment is more costly to install, requiring specialized equipment and safety protocols. Thus, Equation (4) implies a reduction in per kW cost for smaller turbines. Installation costs include lifting, vessels, and handling requirements, and all depend on unit size and mass. The NREL turbine nacelle weighs 100 times more than our turbine, which weighs approximately 3.5 tons [66–68]. A multiplier of 29/4 is applied to our baseline value to account for the difference in the number of turbines.

With similar procedures and common variables, as seen in the previous sections, we utilize the resulting equation, with m_i representing the weight of the nacelle i in tons:

$$C_{m1} = C_{m2} * \frac{m_1}{m_2} * \frac{29}{4} \quad (4)$$

4.3.4. Cost Scaling by the Total Capacity

Finally, we consider how the size of the farm impacts the cost. As the number of units increases, we see the benefit from economies of scale due to shared infrastructure and manufacturing, as described in [69,70]. We use data from the NREL and Sandia [71] and translate the installations into total capacity to estimate the scaling factor for each component, k. This analysis provides estimates for farm sizes with capacity of single-, 10-, 50-, and 100-unit installations.

$$C_{2k} = C_{1k} * (\frac{Q_2}{Q_1})^{x_k} \quad (5)$$

C_{ik} is the cost per kW of component k in design i; Q_i is the capacity of the farm for design i. The exponent, x_k, represents the implicit scaling factor that we estimated from the NREL model for each component k.

First, we used Equation (5) to estimate the scaling factor for each cost component of the NREL reference model. Then, we used these exponents in Equation (5) to estimate the returns to scale in our model. We note that, while the scaling equation assumes a constant exponent (x_k) for every increase in scale, in some cases the NREL cost model resulted in different values of x_k at different deployment scales (e.g., 1–10 units versus 1–50 or 100 units). In these cases, we applied the scale factor that was estimated from the particular case that we were scaling; that is, we used the x_k estimated from scaling 1 to 10 units to estimate the returns to scale for 10 units, and the x_k estimated from scaling 1 to 50 units for that estimate.

4.4. Cost Estimation Results

In this section, we present the results of the cost estimation, including how the cost changes as installed capacity increases. Table 4 summarizes the cost by category for 1-, 3-, and 100-unit installations in \$/kW, illustrating the impact of economies of scale. Figure 6 show how the cost distribution changes with increasing installed capacity. Overall, the proposed system exhibits a high initial capital cost, with a single-unit installation exceeding \$90/W. This is substantially higher than the long-term cost targets for mature renewable energy technologies and is also greater than the estimated cost of the NREL RM4 reference model, which was estimated at \$26/W. The key driver of cost is the relatively small installed capacity due to the depth restriction of the site and number of deployment sites. As deployment scale increases, shared costs are spread over a larger installed capacity, resulting in significant reductions in the cost per kW.

Increasing the number of units installed at one time decreases costs by 43% when going from 1 unit to 3 units, and by 80% for a 100-unit installation. The largest cost reductions occur in Installation, Development, and OPEX, with each subcategory decreasing by more than 85% for the 100-unit case. The Power Take-Off (PTO) and support structure show the smallest reductions in cost. This is due to the limitation on turbine size driven by the shallow depths of the channels. Support Structure costs remain nearly constant on a per-capacity basis as capacity increases, given that this cost is dominated by the cost of steel.

Table 4. Cost breakdown of our model for 1, 3, and 100 units; measured in $/kW.

CAPEX ($/kW)	1-Unit	3-Unit	100-Unit
Power Take-Off	10,819	8846	5049
Installation	4044	1475	199
Support Structure	10,430	9654	8295
Development	59,649	27,984	2412
Contingency	6795	3837	1436
Total	91,737	52,704	17,392
OPEX	1081	9725	2636

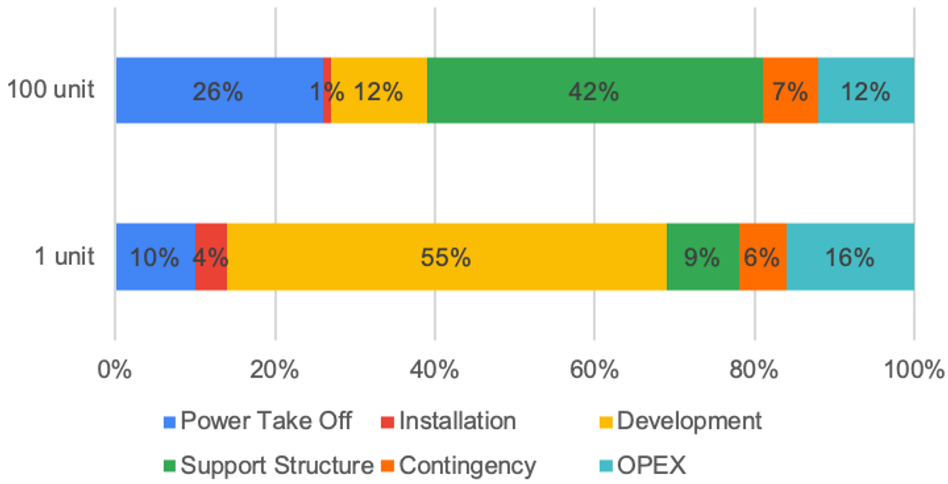

Figure 6. Cost breakdown comparison for 1-unit and 100-unit farm configurations.

5. Levelized Cost of Energy Analysis

5.1. LCOE Estimation Methods

The levelized cost of energy (LCOE) measures the cost per unit energy over a technology's lifetime, accounting for discounting, in $/kWh. This can equivalently be thought of as the break-even price of electricity for the technology. LCOE provides information as a good first estimate of project economic performance and viability, as well as enabling comparisons across technologies [72,73]. The LCOE accounts for the CAPEX, OPEX, and the annual energy production (AEP), as well as the fixed charge rate (FCR), which uses the interest rate and lifetime to convert investment costs into an annual equivalent [74]. CAPEX, OPEX, and the AEP all depend on the location's resource availability and the technology's specifications [75–77].

The LCOE equation is as follows:

$$LCOE = \frac{FCR * CAPEX + OPEX}{AEP} \quad (6)$$

The FCR equation is as follows:

$$FCR = \frac{r(1+r)^t}{(1+r)^t - 1} \quad (7)$$

We assume an interest rate, r, of 7.5%, consistent with the interest rate that the NREL uses for wave energy converters [78]. The lifetime expectancy of the project, t, is 25 years.

5.2. Annual Energy Production

The AEP is the amount of power that a technology produces over the span of one year and is calculated using an hourly time series for data on the currents in the location [79]. The instantaneous power, P, from a turbine (in kW) can be estimated using the following equation [80]:

$$P = \frac{1}{2}\rho C_p \pi R^2 v^3 \tag{8}$$

This equation estimates the average power generated over an hour, given the average hourly velocity, v, in units of m/s. The symbols are as follows: ρ, the density of salt water, 1200 kg/m^3; R, the radius of our turbines, 1.5 m; and Cp, the efficiency of a turbine in converting the energy of current flow into electricity [60]. We assume an actuator disk model for our system, with maximum turbine efficiency at the Betz limit. Thus, we estimate that $C_p = \frac{16}{27}$ [49,81]. We use this model for simplicity; it implies that the efficiency of this technology will be close to the ideal value over time.

A year's worth of velocity data, v, was extracted from the US Caribbean Regional Ocean Modeling System (USCROMS) for each site selected and used to determine resource potential and the AEP calculation.

While this software provides resource assessment of the region of interest, its 2 km horizontal resolution limits its ability to accurately resolve flow magnitudes in narrow channels and shallow coastal regions. Consequently, current velocities extracted from the model likely underestimate the actual current magnitudes for the site. To address this limitation, previous studies recommend applying a correction factor to the current velocity data to account for the underestimation associated with hydrodynamic models. Based on the resolution size of the software and the size of the channels selected, scaling factors ranging from 1.5 to 6 can be applied, as described in [82–84]. We use a current scaling factor of 4 for our case study analysis. While no formal data exists for these locations, this value was selected based on observed current speeds reported by commercial fishing vessels. These vessels use Acoustic Doppler Current Profilers (ADCPs), which can measure the current speeds at various depths. In private communication with the authors, fishermen reported an average current speed of 3 knots, equivalent to 1.5 m/s, within these channels. This figure was used to inform our estimate for the scaling factor. We acknowledge, however, that this value is highly uncertain. Therefore, a sensitivity analysis for the range of current correction factors, 1.5–6, is presented in the results.

Figure 7 shows the hourly velocity over one year with the current correction factor applied. With relatively consistent weather patterns throughout the year, the current velocity is to be fairly consistent year to year. The data had an average current velocity of 1.5 m/s and a maximum velocity at 3.5 m/s. When determining the AEP, we set the cut-in and cut-out speed to be 0.8 m/s and 4.0 m/s, respectively. All three sites show similar trends in variance. This can be useful when looking at future supply and demand needs over a 24 h period for the island.

5.3. LCOE Results

Table 5 shows the LCOE calculated for 1-, 3-, 10-, 50-, and 100-unit installations. For small deployments, the LCOE remains substantially higher than present electricity prices, reaching \$2.02/kWh for a single-unit system. LCOE reduces by 44% when using all three sites within our case study, with an LCOE of \$1.13/kWh. As the number of units increases to 50-unit farms, we see the LCOE decrease by 81%, reaching competitive costs of \$0.38/kWh. While the LCOE continues to decrease beyond 50 units, the rate of reduction slows. Figure 8 illustrates that this technology achieves break-even cost compared with the existing electricity rate in the US Virgin Islands at an installed capacity of approximately

10 MW [85]. This implies that about 41 installed units would be required to meet this threshold. Thus, these results suggest that economic viability is achievable on medium- to large-scale deployment.

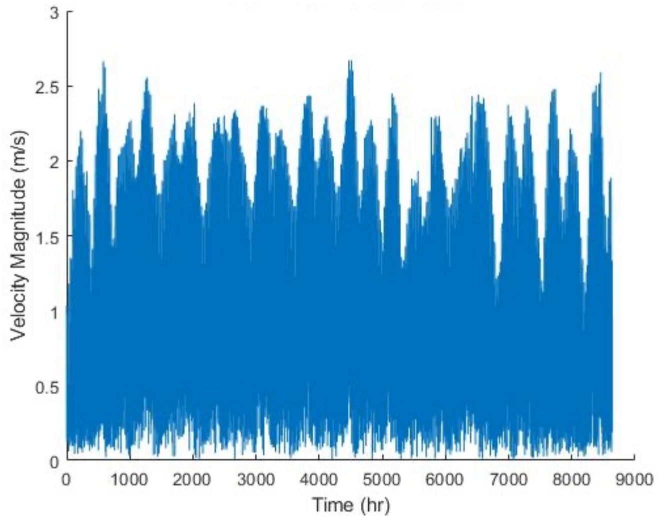

Figure 7. Current speed data in m/s over one year taken from the USCROMS model for the site, with a current correction factor of 4.

Table 5. Levelized cost of energy (LCOE) for production/installation of 1–100 units.

Number of Units	Capacity (kW)	LCOE ($/kWh)
1-unit	240	$2.02
3-unit	719	$1.13
10-unit	2397	$0.66
50-unit	11,983	$0.38
100-unit	23,967	$0.31

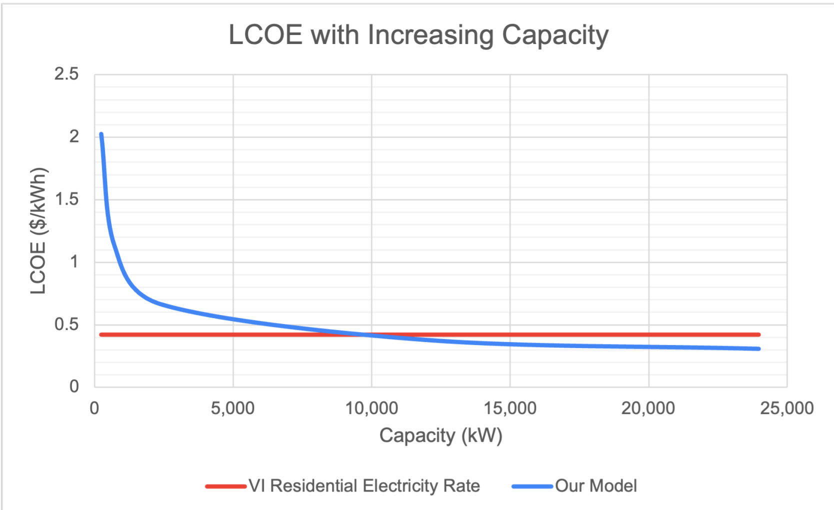

Figure 8. LCOE as capacity of the farm increases, compared to the existing residential cost of electricity in the USVI, rating at 0.42 $/kWh.

We note that the LCOE is a not a perfect measure, as it does not account for issues around intermittency: many papers have pointed out that total system costs are different for intermittent and non-dispatchable technologies [86,87]. The LCOE also has limitations in fully capturing the costs that translate to the residential consumer. According to the Water and Power Authority's electric rate breakdown, retail electric rates are primarily driven by direct fuel costs, at \$0.22/kWh, and residential energy charges, at \$0.18/kWh. The residential energy charges include capital costs through debt service, equipment repairs, and annual insurance, along with transmission and distribution. Our LCOE estimate captures capital costs and OPEX (i.e., equipment repairs, insurance, etc.) but does not capture transmission or distribution. There is no data available for these costs. Therefore, we use the reported residential cost of \$0.42/kWh as a comparison in Figure 8, but we acknowledge that the real break-even cost will be lower once distribution costs are accounted for.

5.4. Sensitivity Analysis

We identified three main components that impact the LCOE of the proposed technology: the current correction factor; the depth of the channel, which determines the size of the turbines and their corresponding number; and the interest rate for the project. A sensitivity analysis was conducted for each of these to evaluate the impact on project economics, identify the most influential parameters, and assess pathways for improving economic viability.

5.4.1. Current Correction Factor

As detailed in Section 5.2, current correction factors ranging from 1.5 to 6 can be applied to the resource velocity extracted from the model, because of the large resolution size of the USCROMS model (2 km) compared to our channel size of 150 m. This range was selected based on these sources, which showed at least a 50% increase in resources within channels and a high estimate of six times the current estimated from ocean modeling software [82–84]. The current speed plays a major role in reducing the LCOE for this study, from \$1.14/kWh under our central assumption of 4 to \$0.50/kWh under a multiplier of 6 (See Figure 9).

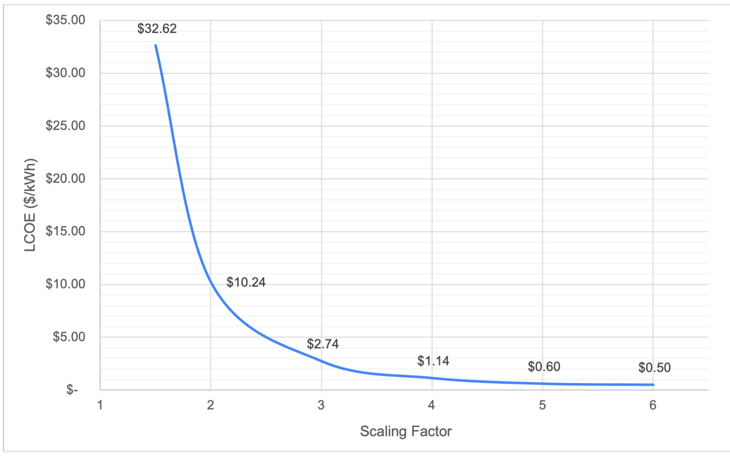

Figure 9. Sensitivity of the LCOE for a 3-unit case, in \$/kWh, for current correction factors ranging from 1.5 to 6.

5.4.2. LCOE vs. Depth Restrictions

The depth of the channel restricts the turbine size. Here, we investigate how the resulting turbine size impacts the LCOE. As we change the turbine size, we also change the number of turbines per unit. The rotor diameter ranges from 2 m to 33 m, with the number of turbines selected using the packing and power optimization as shown in Equation (9):

$$N = \frac{L}{kD} \tag{9}$$

- L—Bridge length;
- k—Spacing factor;
- D—Turbine diameter.

This equation is a standard geometric packing relationship based on the bridge length and the spacing factor. According to [88–90], side-by-side arrangements of tidal turbines can have a center-to-center spacing of 1.5–3 rotor diameters. This is to reduce the wake effects and blockage ratio of the system, which can drastically reduce the mechanical efficiency of a project. We assume a 1.72D for turbine rotors 2 and 3 m in diameter and increase to 2D for diameters of 4–15 m, as larger turbines can expect larger wake effects. Figure 10 shows that, as the depth of the channel increases, the larger rotor diameter leads to a smaller number of turbines per unit (as measured on the right axis). In turn, these fewer, larger turbines generate more energy; thus, the LCOE decreases with depth. Based on this analysis, three sites with an average depth of 18–20 m could accommodate eight 9–10 m diameter turbines and achieve break-even LCOE in the USVI. For the 33 m, NREL RM4 turbine, a depth requirement of 65–70 m would be necessary to accommodate one of their units. This scenario highlights the importance of turbine sizing and installed capacity in improving project economics.

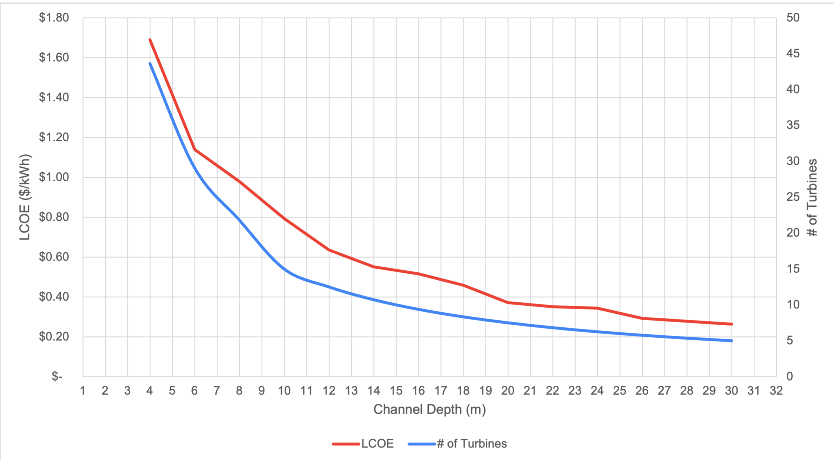

Figure 10. Impact of channel depth on the optimal number of turbines and the LCOE. The red line shows the LCOE for a 3-unit farm, which can be read on the left vertical axis; the blue line is the optimal number of turbines per unit as a function of the rotor diameter, which can be read on the right vertical axis.

5.4.3. Interest Rate

The interest rate (r) value of 7.5% used in our baseline LCOE estimate is taken from the NREL study. However, the interest rate for renewable energy projects, particularly in the SIDS, can vary greatly due to local development, permitting and regulatory frameworks, and the perceived investment risk within marine energy technologies [91,92]. To address this volatility of interest rate estimates and the impact on the LCOE results, we illustrate the LCOE as a function of the interest rate, 2–20%, for a 3-unit and 100-unit farm. Figure 11 show how the interest rate impacts the LCOE. The interest rate is used in the Equation (7) and represents the cost of capital and perceived investment risk associated with a project. As the interest rate increases, annualized costs increase, resulting in a higher LCOE.

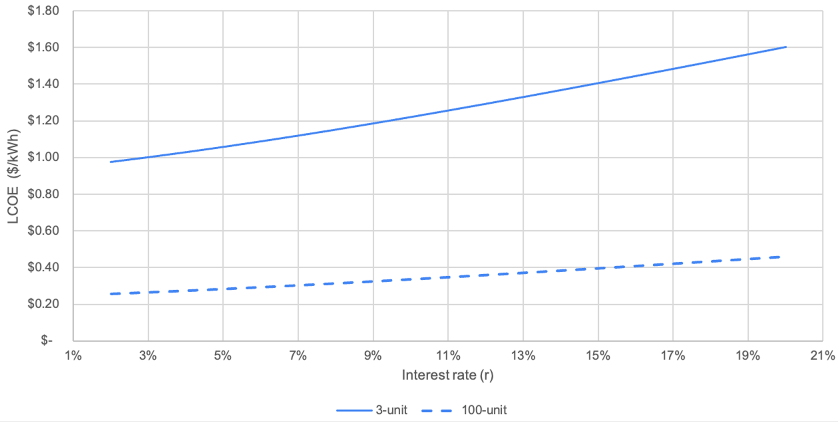

Figure 11. LCOE in $/kWh as a function of the interest rate.

6. Discussion and Conclusions

The goal of this study was to evaluate the techno-economic feasibility of applying tidal energy technologies to the U.S. Virgin Islands and other Caribbean island regions. The results indicate that the economic viability of this marine hydrokinetic technology within the US Virgin Islands and other SIDS is primarily driven by economies of scale. A 1-unit farm using our proposed bridge structure located in a shallow channel has a rated capacity of 239 kW and an LCOE of $2.02/kWh, making small-unit deployment economically unrealistic. However, the LCOE decreases substantially as the number of units increases, resulting in the technology achieving a break-even cost in the U.S. Virgin Islands at an installed capacity of 10 MW. This suggests that the technology is best suited for coordinated multi-unit deployments, both locally and across other island nations.

There are opportunities for large-scale installation within the USVI and across the Caribbean. Around the Virgin Islands there are 100 smaller surrounding land masses, implying the possibility of large-scale installation across the territory. In addition, the geographic proximity of many SIDS in Caribbean archipelagos presents opportunities for coordinated development of larger marine energy installations across multiple sites, and the bridge structures may allow for inter-island connection. Thus, achieving large deployment scales may be possible through regional collaboration. In fact, international initiatives are increasingly supporting shared renewable energy project deployment. Examples of existing initiatives include the U.S.–Caribbean partnership to Address the Climate Crisis 2030, led by the US Department of State; and the Caribbean Resilient Renewable Energy Infrastructure Investment Facility, supported by the World Bank [6,93].

The easily accessible bridge support structure proposed in this study can increase the opportunity for widespread development in the SIDS due to ease of access, removing the need for special machinery to perform installation and regular maintenance. The bridge-supported structure can also create opportunities for local labor participation during construction and maintenance, which can increase energy resilience and autonomy [94–96]. Future work could include simulating structural stability using concrete or wood, which can be locally sourced across different SIDS.

The depth of the channels has a substantial influence on project viability, as larger turbines increase energy production while reducing the number of units. Our results indicate that this bridge design would achieve break-even with USVI prices at water depths of 18–20 m with only three units installed. This compares to the minimum required depth of 65–70 m for the floating RM4 to be installed. In general, our bridge-supported marine concept targets shallow, narrow channel environments, extending marine energy opportunities to locations where they may not have been previously feasible. We note that this marine energy system may incur some negative environmental and social impacts.

Construction and fabrication may have coastal environmental impacts. Another concern is that the bridge structure may prevent some economic or recreational uses of the channels. The channels selected are not passable by major commercial vessels or barges (i.e., cruise ships, ferries, tugboats, etc.) but can be traveled by smaller vessels that are used for fishing or recreation. A more thorough assessment should incorporate environmental studies and engagement with local maritime communities, along with other stakeholders, to ensure that the proposed installations are compatible with existing uses of the marine environment.

We also want to highlight that, while the proposed turbine spacing meets the minimum recommended values and is effective as a preliminary assessment, the cumulative wake effects and the resulting blockage ratio are not fully captured, particularly for the simultaneous operation of 29 turbines in a narrow channel. Garrett and Cummins have illustrated how the resulting turbine efficiency can decrease as the blockage ratio approaches 1 [49]. Recent studies show that, in offshore wind energy, benchmark models can effectively be used for evaluating the dynamic response of these technologies, while data-driven approaches can be used for event-triggered analysis, thus improving the validation and reproducibility of these types of offshore renewable energy systems [97,98]. Similar analysis frameworks could be extended to our system for evaluating the turbine performance and structural response to these high-density, narrow channel environments.

There are a number of uncertainties in the cost assumptions derived from NREL reference models. While these reference models provide a valuable and widely accepted foundation for cost estimation and scaling analyses, future reductions in capital costs are expected as marine energy technologies mature. For Equations (2) and (5), these are standard scaling equations, widely used in the literature. Nevertheless, there can be aspects that are hard to model in reality. Equation (3) is based on the assumption that fixed costs are spread out across the entire project. Equation (4) is the most speculative; it is based on our assumptions about how costs scale with the mass of the turbine. Future work could examine this more closely if data is available about installation costs. In addition to this, NREL estimates may not fully capture location-specific costs associated with energy deployment in the SIDS. Local cost premiums may increase the estimated costs of this technology, due to import requirements, lack of policy and regulatory frameworks, and local supply-chain constraints [99–102]. Continued technology development, deployment experience, supply-chain growth, and manufacturing improvements are likely to lead to lower costs as the technology is deployed [91,103–105]. Examples of global policy initiatives that can financially aid in renewable energy project developments include green and blue bonds [106]. Green bonds provide low-cost funding for projects that promote environmental sustainability, and blue bonds are an extension of this for marine conservation projects.

Renewable energy transition continues to be challenging across the globe, but it is especially daunting to locations like the US Virgin Islands and other Small Island Developing States, who share common environmental and economic circumstances. This research highlights the potential of marine current technology as a renewable resource that leverages unique channelized flow conditions throughout many island regions. By simplifying installation and maintenance while leveraging existing bridge infrastructure, the proposed concept addresses several barriers that have historically limited marine current energy development for Small Island Developing States and globally. These findings provide a foundation for future research and demonstrate the potential role of innovative support structures in expanding renewable energy opportunities for islands and coastal communities. Furthermore, this research emphasizes local participation in site selection, project development, operation, and maintenance, supporting long-term energy sustainability, resilience, and community engagement.

Author Contributions: Conceptualization, J.A.; Methodology, J.A.; Validation, J.A. and E.B.; Formal analysis, J.A.; Investigation, J.A.; Resources, J.A.; Writing—original draft, J.A.; Writing—review & editing, J.A. and E.B.; Visualization, J.A.; Supervision, E.B.; Project administration, E.B.; Funding acquisition, E.B. All authors have read and agreed to the published version of the manuscript.

Funding: This research was funded in part by work initially supported by NSF Grant 2021693, and continuing support from the Massachusetts Clean Energy Center Workforce Development Program. This work was also funded by the Switzer Foundation.

Data Availability Statement: The raw data supporting the conclusions of this article will be made available by the authors on request.

Acknowledgments: The authors would like to acknowledge the support of the University of the Virgin Islands for providing access to the current velocity data that made validating the AEP possible. We would also like to thank the local fishing community for providing guidance and support in the idea of developing a marine energy project within the territory.

Conflicts of Interest: The authors declare no conflicts of interest.

Abbreviations

The following abbreviations are used in this manuscript:

SIDS	Small Island Developing States
LCOE	Levelized Cost of Energy
NREL	National Lab of the Rockies (formally National Renewable Energy Lab)
CAPEX	Capital Expenditures
OPEX	Operation Expenditures
AEP	Annual Energy Production
O&M	Operation and Maintenance
USVI	United States Virgin Islands
NOAA	National Oceanic and Atmospheric Administration
USCROMS	US Caribbean Ocean Modeling System
PTO	Power Take-Off

Appendix A

Equation (2): Scaling for how the cost is impacted by the rotor radius is linear; however, it is based on the power equation, which is quadratic. Here, we derive the final equation. First, we note the following relationship, as the cost of materials will increase proportionally as the radius gets larger, but the cost per unit power will decrease proportionately with the power:

$$C_{r_1} = C_{r_2} \frac{r_1}{r_2} \frac{P_2}{P_1} \tag{A1}$$

By substituting Equation (8) to the above, the resulting equation is

$$C_{r_1} = C_{r_2} \frac{r_1}{r_2} \frac{r_2^2}{r_1^2} \tag{A2}$$

This simplifies to our Equation (2).

References

1. Mycoo, M.; Wairiu, M.; Campbell, D.; Duvat, V.; Golbuu, Y.; Maharaj, S.; Nalau, J.; Nunn, P.; Pinnegar, J.; Warrick, O. *Small Islands*; Cambridge University Press: Cambridge, UK, 2022.
2. International Renewable Energy Agency (IRENA). *Ocean Energy: Technologies, Patents, Deployment Status and Outlook*; International Renewable Energy Agency: Abu Dhabi, United Arab Emirates, 2014. Available online: https://www.irena.org/publications/2014/Aug/Ocean-Energy-Technologies-Patents-Deployment-Status-and-Outlook (accessed on 31 July 2023).

3. Bir, G.S.; Lawson, M.J.; Li, Y. Structural design of a horizontal-axis tidal current turbine composite blade. *Proc. Int. Conf. Offshore Mech. Arct. Eng.* **2011**, *44373*, 797–808. [CrossRef]
4. Roberts, S.; Lewis-Cameron, A. Small island developing states: Issues and prospects. In *Marketing Island Destinations*; Routledge: Oxfordshire, UK, 2010; pp. 1–10.
5. The Economist. *The Caribbean Struggles to Break Its Dependence on Fossil Fuels*; The Economist: London, UK, 2024. Available online: https://www.economist.com/the-americas/2024/12/12/the-caribbean-struggles-to-break-its-dependence-on-fossil-fuels (accessed on 7 January 2026).
6. World Bank. *Caribbean Countries Move Toward Energy Sustainability with New Regional Project*; World Bank: Washington, DC, USA, 2025. Available online: https://www.worldbank.org/en/news/press-release/2025/03/04/caribbean-countries-move-toward-energy-sustainability-with-new-regional-project (accessed on 19 March 2025).
7. Vousdoukas, M.I.; Athanasiou, P.; Giardino, A.; Mentaschi, L.; Stocchino, A.; Kopp, R.E.; Menéndez, P.; Beck, M.W.; Ranasinghe, R.; Feyen, L. Small Island Developing States under threat by rising seas even in a 1.5 C warming world. *Nat. Sustain.* **2023**, *6*, 1552–1564. [CrossRef]
8. Thomas, A.; Baptiste, A.; Martyr-Koller, R.; Pringle, P.; Rhiney, K. Climate Change and Small Island Developing States. *Annu. Rev. Environ. Resour.* **2020**, *45*, 1–27. [CrossRef]
9. Pelling, M.; Uitto, J.I. Small island developing states: Natural disaster vulnerability and global change. *Glob. Environ. Change Part B Environ. Hazards* **2001**, *3*, 49–62. [CrossRef]
10. Niles, K.; Lloyd, B. Small Island Developing States (SIDS) & energy aid: Impacts on the energy sector in the Caribbean and Pacific. *Energy Sustain. Dev.* **2013**, *17*, 521–530. [CrossRef]
11. Robinson, M. The Debt Experience of SIDS in the Caribbean. In *Debt and Development in Small Island Developing States*; King, D., Tennant, D.F., Eds.; Palgrave Macmillan: New York, NY, USA, 2014; pp. 29–69. [CrossRef] [PubMed]
12. Denny, E. The economics of tidal energy. *Energy Policy* **2009**, *37*, 1914–1924. [CrossRef]
13. Roberts, A.; Thomas, B.; Sewell, P.; Khan, Z.; Balmain, S.; Gillman, J. Current tidal power technologies and their suitability for applications in coastal and marine areas. *J. Ocean. Eng. Mar. Energy* **2016**, *2*, 227–245. [CrossRef]
14. Lewis, M.; Neill, S.; Robins, P.; Hashemi, M.R. Resource assessment for future generations of tidal-stream energy arrays. *Energy* **2015**, *83*, 403–415. [CrossRef]
15. Wardell, C.; Huvenne, V.A. Broadscale landscape mapping provides insight into the Commonwealth of Dominica and surrounding islands offshore environment. *Remote Sens.* **2022**, *14*, 1820. [CrossRef]
16. U.S. National Centers for Environmental Information. NOAA Bathymetry Maps. 2026. Available online: https://www.ncei.noaa.gov/maps/bathymetry/ (accessed on 22 January 2026).
17. Segura, E.; Morales, R.; Somolinos, J.A. Cost assessment methodology and economic viability of tidal energy projects. *Energies* **2017**, *10*, 1806. [CrossRef]
18. Zupone, G.L.; Amelio, M.; Barbarelli, S.; Florio, G.; Scornaienchi, N.M.; Cutrupi, A. Lcoe evaluation for a tidal kinetic self balancing turbine: Case study and comparison. *Appl. Energy* **2017**, *185*, 1292–1302. [CrossRef]
19. Thiébot, J.; Sedrati, M.; Guillou, S. The Potential of Tidal Energy Production in a Narrow Channel: The Gulf of Morbihan. *J. Mar. Sci. Eng.* **2024**, *12*, 479. [CrossRef]
20. Ross, H.; Polagye, B. An experimental assessment of analytical blockage corrections for turbines. *Renew. Energy* **2020**, *152*, 1328–1341. [CrossRef]
21. Thake, J. Development, Installation and Testing of a Large-Scale Tidal Current Turbine. 2005. Available online: https://www.osti.gov/etdeweb/servlets/purl/20714897 (accessed on 11 September 2026).
22. Astariz, S.; Vazquez, A.; Iglesias, G. Evaluation and comparison of the levelized cost of tidal, wave, and offshore wind energy. *J. Renew. Sustain. Energy* **2015**, *7*, 053112. [CrossRef]
23. McDowell, J.A.; Marine, P.J.S. Levelised Cost of Energy Site Selection Tool for Tidal Stream Energy Devices. Ph.D. Thesis, University of Edinburgh, Edinburgh, UK, 2021.
24. Zhang, D.; Yang, K.; Zhang, H.; Yang, K.; Zeng, S.; Si, K.; Zhang, Y. Challenges in tidal energy commercialization and technological advancements for sustainable solutions. *iScience* **2025**, *28*, 112348. [CrossRef] [PubMed]
25. Kumar, A.; Hayatdavoodi, M. On wave–current interaction in deep and finite water depths. *J. Ocean. Eng. Mar. Energy* **2023**, *9*, 455–475. [CrossRef]
26. Biggs, H.; Smart, G.; Doyle, M.; Eickelberg, N.; Aberle, J.; Randall, M.; Detert, M. Surface velocity to depth-averaged velocity—A review of methods to estimate alpha and remaining challenges. *Water* **2023**, *15*, 3711. [CrossRef]
27. Olis, D.; Leddy, L. *U.S. Virgin Islands 2023 Energy Baseline Report*; Technical Report NREL/TP-7A40-88770; National Renewable Energy Laboratory: Applewood, CO, USA, 2024.
28. Choose Energy. Electricity Rates by State. 2026. Available online: https://www.electricchoice.com/electricity-prices-by-state/ (accessed on 11 September 2026).

29. Virgin Islands Water and Power Authority. Megawatt Hours Production Report: May 2026. Excel Spreadsheet. 2026. Available online: https://www.viwapa.vi/customer-service/megawatt-hours-production-report (accessed on 1 June 2026).
30. Bates, A.; Guannel, G.; Quinones, L.A.P. Hurricanes make headlines, but chronic utility failure drives energy (in) security in the US Virgin Islands. *Energy Policy* **2024**, *195*, 114320. [CrossRef]
31. U.S. Energy Information Administration. *U.S. Virgin Islands Energy Profile and Analysis*; U.S. Energy Information Administration: Washington, DC, USA, 2026.
32. Martin-Short, R.; Hill, J.; Kramer, S.; Avdis, A.; Allison, P.; Piggott, M. Tidal resource extraction in the Pentland Firth, UK: Potential impacts on flow regime and sediment transport in the Inner Sound of Stroma. *Renew. Energy* **2015**, *76*, 596–607. [CrossRef]
33. Ghefiri, K.; Garrido, A.J.; Rusu, E.; Bouallègue, S.; Haggège, J.; Garrido, I. Fuzzy supervision based-pitch angle control of a tidal stream generator for a disturbed tidal input. *Energies* **2018**, *11*, 2989. [CrossRef]
34. Neary, V.; Lawson, M.; Li, Y.; Sale, D.; Fontaine, A.; Beam, M.; Kline, B.; Epler, J.; Previsic, M.; Shoele, K.; et al. *Reference Model 4 Full Scale Geometry (RM4: Ocean Current Turbine)*; Marine and Hydrokinetic Data Repository, Sandia National Laboratories: Albuquerque, NM, USA, 2014. [CrossRef]
35. U.S. National Oceanic and Atmospheric Administration. *NOAA Custom Chart*; Office of Coast Survey: Silver Spring, MD, USA, 2025. Available online: https://devgis.charttools.noaa.gov/pod/ (accessed on 8 April 2025).
36. Mukherjee, S.; Habtes, S.; Jobsis, P. Comparative analysis of the performance of the GOFS, PSY4 and AMSEAS ocean model frameworks in the Virgin Islands and Puerto Rico coastal ocean. *J. Oper. Oceanogr.* **2023**, *16*, 211–235. [CrossRef]
37. Mukherjee, S.; Wilson, D.; Jobsis, P.; Habtes, S. Numerical modeling of internal tides and submesoscale turbulence in the US Caribbean regional ocean. *Sci. Rep.* **2023**, *13*, 1. [CrossRef] [PubMed]
38. Jenne, D.S.; Yu, Y.H.; Neary, V. *Levelized Cost of Energy Analysis of Marine and Hydrokinetic Reference Models*; Technical Report; National Renewable Energy Lab. (NREL): Golden, CO, USA, 2015.
39. Neary, V.; Lawson, M.; Li, Y.; Sale, D.; Fontaine, A.; Beam, M.; Kline, B.; Epler, J.; Previsic, M.; Polagye, B. *Reference Model 1 Full Scale Geometry (RM1: Tidal Current Turbine)*; Technical Report, Marine and Hydrokinetic Data Repository (MHKDR); Sandia National Laboratories: Albuquerque, MN, USA, 2014.
40. Neary, V.S.; Lawson, M.; Previsic, M.; Copping, A.; Hallett, K.C.; Labonte, A.; Rieks, J.; Murray, D. *Methodology for Design and Economic Analysis of Marine Energy Conversion (MEC) Technologies*; Sandia National Lab. (SNL-NM): Albuquerque, NM, USA, 2014.
41. Jiang, H.R.; Bai, X.L.; Vaz, M.A. Aero-hydrodynamic coupled dynamic characteristics of semi-submersible floating offshore wind turbines under inflow turbulence. *China Ocean. Eng.* **2023**, *37*, 660–672. [CrossRef]
42. Micallef, D.; Rezaeiha, A. Floating offshore wind turbine aerodynamics: Trends and future challenges. *Renew. Sustain. Energy Rev.* **2021**, *152*, 111696. [CrossRef]
43. Barbarelli, S.; Florio, G.; Amelio, M.; Scornaienchi, N.; Cutrupi, A.; Zupone, G.L. Transients analysis of a tidal currents self-balancing kinetic turbine with floating stabilizer. *Appl. Energy* **2015**, *160*, 715–727. [CrossRef]
44. Coles, D.S.; Mackie, L.; White, D.; Miles, J. Cost Modelling and Design Optimisation of Tidal Stream Turbines. 2021. Available online: https://interregtiger.com/download/research-paper-cost-modelling-and-design-optimisation-of-tidal-stream-turbine/ (accessed on 11 September 2026).
45. Zhang, C.; Zhang, K.; Cheng, X.; Lin, X.; Zhang, J.; Wu, C.; Ren, Z. Investigating tidal stream turbine array performance considering effects of number of turbines, array layouts, and yaw angles. *J. Mar. Sci. Eng.* **2024**, *12*, 2325. [CrossRef]
46. Henzan, K.; Furue, T.; Matsunari, I. Challenges Toward Commercializing Tidal Power Technology: Outcomes and Prospects from Japan's First Large-Scale Demonstration Project. In *Proceedings of the 2024 13th International Conference on Renewable Energy Research and Applications (ICRERA)*; IEEE: Piscataway, NJ, USA, 2024; pp. 774–776.
47. Johnstone, C.; Pratt, D.; Clarke, J.; Grant, A. A techno-economic analysis of tidal energy technology. *Renew. Energy* **2013**, *49*, 101–106. [CrossRef]
48. Nautical Charts App/GPS Nautical Charts. Virgin Islands: Virgin Gorda to St. Thomas and St. Croix Marine Chart (CB_US25641_P386). Marine Navigation Chart Derived from Official Hydrographic Data, Including Bathymetry and Channel Information for the US Virgin Islands. 2025. Available online: https://fishing-app.gpsnauticalcharts.com/i-boating-fishing-web-app/fishing-marine-charts-navigation.html?title=VIRGIN+ISLANDS+VIRGIN+GORDA+TO+ST+THOMAS+AND+ST+CROIX+boating+app#13.67/18.3541/-65.0435 (accessed on 11 September 2026).
49. Garrett, C.; Cummins, P. The efficiency of a turbine in a tidal channel. *J. Fluid Mech.* **2007**, *588*, 243–251. [CrossRef]
50. Garrett, C.; Cummins, P. The power potential of tidal currents in channels. *Proc. R. Soc. A Math. Phys. Eng. Sci.* **2005**, *461*, 2563–2572. [CrossRef]
51. Chen, W.F.; Duan, L. *Bridge Engineering Handbook, Second Edition: Superstructure Design*, 2nd ed.; CRC Press: Boca Raton, FL, USA, 2014.
52. Barker, R.M.; Puckett, J.A. (Eds.) *Design of Highway Bridges: An LRFD Approach*, 2nd ed.; Wiley: Hoboken, NJ, USA, 2007. [CrossRef]

53. StructuralBasics.com. The Pratt Truss Explained [2025]. StructuralBasics.com. 2025. Available online: https://www.structuralbasics.com/pratt-truss/ (accessed on 23 April 2025).
54. American Institute of Steel Construction. *Steel Construction Manual | American Institute of Steel Construction*, 16th ed.; American Institute of Steel Construction: Chicago, IL, USA, 2025. Available online: https://books.google.com/books?hl=en&lr=&id=wfzTAAAAQBAJ&oi=fnd&pg=PA8&dq=16th+ed.+Steel+Construction+Manual&ots=E8BT3mVMP4&sig=_5go9oqsh-uONjmWNqTkBvD5M90#v=onepage&q&f=false (accessed on 14 May 2025).
55. Raikwar, A.; Ahmed, S.; Warudkar, V. Analytical displacement model of wind turbine towers under loading conditions. *Int. Res. J. Adv. Sci. Hub.* **2021**, *3*, 90–100. [CrossRef]
56. Polagye, B.; Previsic, M.; Bedard, R. *System Level Design, Performance, Cost and Economic Assessment: Knik Arm Alaska Tidal In-Stream Power Plant*; EPRI: Palo Alto, CA, USA, 2006. Available online: https://www.re-vision.net/documents/System%20Level%20Design,%20Performance,%20Cost%20and%20Economic%20Assessment%20-%20Alaska%20River%20In-Stream%20Power%20Plants.pdf (accessed on 11 September 2026).
57. Previsic, M.; Chozas, J. *International Levelised Cost of Energy for Ocean Energy Technologies*; Ocean Energy Systems: Paris, France, 2015; pp. 1–48.
58. Shetty, C.; Priyam, A. A review on tidal energy technologies. *Mater. Today Proc.* **2022**, *56*, 2774–2779. [CrossRef]
59. Egli, F.; Steffen, B.; Schmidt, T.S. *12 Cost of Capital for Renewable Energy: The Role of Industry Experience and Future Potentials*; Green Banking: Washington, DC, USA, 2020; pp. 335–348.
60. ScienceDirect Topics. *Power Coefficient—An Overview*; ScienceDirect: Amsterdam, The Netherlands, 2024. Available online: https://www.sciencedirect.com/topics/engineering/power-coefficient (accessed on 24 January 2024).
61. Renotag. *How Much Does A Steel Beam Cost to Install?* Renotag: Calgary, AB, Canada, 2025. Available online: https://renotag.com/costs/steel-beam-cost-to-install/ (accessed on 12 June 2025).
62. Reis, A.; Pedro, J. *Bridge Design: Concepts and Analysis*; John Wiley & Sons: Hoboken, NJ, USA, 2019. [CrossRef]
63. Nebraska Department of Transportation. *State Bridge Summary*; Nebraska Department of Transportation: Lincoln, NE, USA, 2012. Available online: https://dot.nebraska.gov/media/ztelbmic/state_bridge_summary_2012.pdf (accessed on 11 September 2026).
64. Hadi, M.; Orabi, W.; Xiao, Y.; Ibrahim, M.; Jia, J. Estimating Total Cost of Bridge Construction Using ABC and Conventional Methods of Construction. 2017. Available online: https://rosap.ntl.bts.gov/view/dot/42743 (accessed on 11 September 2026).
65. Assets, I.B. Bridge Bundling Guidebook. 2019. Available online: https://abc-utc.fiu.edu/wp-content/uploads/2020/05/2019_10-17_FHWA_BBG_Presentation_toHPA_CLEARED.pdf (accessed on 11 September 2026).
66. Bahaj, A.S. Generating electricity from the oceans. *Renew. Sustain. Energy Rev.* **2011**, *15*, 3399–3416. [CrossRef]
67. Tethys Engineering, Pacific Northwest National Laboratory. *Tidal Energy: Technology Brief*; Tethys Engineering: Richland, WA, USA, 2025. Available online: https://tethys-engineering.pnnl.gov/publications/tidal-energy-technology-brief (accessed on 24 June 2025).
68. Myers, L.; Bahaj, A.S. Simulated electrical power potential harnessed by marine current turbine arrays in the Alderney Race. *Renew. Energy* **2005**, *30*, 1713–1731. [CrossRef]
69. Key, A.; Roberts, O.; Eberle, A. Scaling trends for balance-of-system costs at land-based wind power plants: Opportunities for innovations in foundation and erection. *Wind Eng.* **2022**, *46*, 896–913. [CrossRef]
70. Shields, M.; Beiter, P.; Nunemaker, J.; Cooperman, A.; Duffy, P. Impacts of turbine and plant upsizing on the levelized cost of energy for offshore wind. *Appl. Energy* **2021**, *298*, 117189. [CrossRef]
71. Neary, V.S.; Kobos, P.H.; Jenne, D.S.; Yu, Y.H. *Levelized Cost of Energy for Marine Energy Conversion (MEC) Technologies*; Technical Report; Sandia National Lab. (SNL-NM): Albuquerque, NM, USA, 2016.
72. IEA; NEA. *Projected Costs of Generating Electricity*; OECD Publishing: Paris, France, 2020.
73. Brown, T.; Reichenberg, L. Decreasing market value of variable renewables is a result of policy, not variability. *arXiv* **2020**, arXiv:2002.05209.
74. Mai, T.; Mowers, M.; Eurek, K. *Competitiveness Metrics for Electricity System Technologies*; Technical Report; National Renewable Energy Lab. (NREL): Golden, CO, USA, 2021. Available online: https://docs.nlr.gov/docs/fy21osti/72549.pdf (accessed on 11 September 2026).
75. Ueckerdt, F.; Hirth, L.; Luderer, G.; Edenhofer, O. System LCOE: What are the costs of variable renewables? *Energy* **2013**, *63*, 61–75. [CrossRef]
76. Cory, K.; Schwabe, P. *Wind Levelized Cost of Energy: A Comparison of Technical and Financing Input Variables*; Technical Report NREL/TP-6A2-46671; National Renewable Energy Laboratory (NREL): Golden, CO, USA, 2009. [CrossRef] [PubMed]
77. Kalowekamo, J.; Baker, E. Estimating the manufacturing cost of purely organic solar cells. *Sol. Energy* **2009**, *83*, 1224–1231. [CrossRef]
78. Baca, E.; Philip, R.; Greene, D.; Battey, H. *Expert Elicitation for Wave Energy LCOE Futures*; Technical Report NREL/TP-5700-82375; National Renewable Energy Laboratory (NREL): Golden, CO, USA, 2022. [CrossRef]

79. ScienceDirect Topics. *Annual Energy Production—An Overview*; ScienceDirect: Amsterdam, The Netherlands, 2024. Available online: https://www.sciencedirect.com/topics/engineering/annual-energy-production (accessed on 15 January 2024).
80. Manwell, J.F.; McGowan, J.G.; Rogers, A.L. *Wind Energy Explained: Theory, Design and Application*; John Wiley & Sons: Hoboken, NJ, USA, 2010.
81. Bergey, K.H. The Lanchester-Betz limit (energy conversion efficiency factor for windmills). *J. Energy* **1979**, *3*, 382–384. [CrossRef]
82. Yang, X.; Haas, K.A. Improving assessments of tidal power potential using grid refinement in the Coupled Ocean-Atmosphere-Wave-Sediment Transport model. *J. Renew. Sustain. Energy* **2015**, *7*, 043107. [CrossRef]
83. Wang, X.; Chao, Y.; Li, Z.; Dong, C.; Farrara, J.; McWilliams, J.C.; Shum, C.; Wang, Y.; Matsumoto, K.; Rosenfeld, L.K.; et al. Tidal Simulation Using Regional Ocean Modeling Systems (ROMS). 2006. Available online: https://www.academia.edu/download/39582978/TIDAL_SIMULATION_USING_REGIONAL_OCEAN_MO20151101-23635-mk5ouh.pdf (accessed on 11 September 2026).
84. Wang, T.; Yang, Z. A Tidal Hydrodynamic Model for Cook Inlet, Alaska, to Support Tidal Energy Resource Characterization. *J. Mar. Sci. Eng.* **2020**, *8*, 254. [CrossRef]
85. Virgin Islands Water and Power Authority. About WAPA. 2025. Available online: https://www.viwapa.vi/about-us (accessed on 2 June 2025).
86. Joskow, P.L. Comparing the costs of intermittent and dispatchable electricity generating technologies. *Am. Econ. Rev.* **2011**, *101*, 238–241. [CrossRef]
87. Idel, R. Levelized full system costs of electricity. *Energy* **2022**, *259*, 124905. [CrossRef]
88. Myers, L.E.; Bahaj, A.S. Wake studies of a horizontal axis marine current turbine. *Proc. Inst. Mech. Eng. Part A* **2007**, *221*, 171–181.
89. Malki, R.; Williams, A.J.; Croft, T.N. Planning tidal stream turbine array layouts using a coupled blade element momentum computational fluid dynamics model. *Renew. Energy* **2014**, *63*, 46–54. [CrossRef]
90. Funke, S.W.; Farrell, P.E.; Piggott, M.D. Tidal turbine array optimisation using the adjoint approach. *Renew. Energy* **2014**, *63*, 658–673. [CrossRef]
91. International Renewable Energy Agency. *Renewable Power Generation Costs in 2024*; Technical Report; International Renewable Energy Agency: Abu Dhabi, United Arab Emirates, 2025.
92. Jena, L.P.; Chaturvedi, A. Renewable energy financing in the Pacific Island Countries. *Energy Sustain. Dev.* **2025**, *85*, 101642. [CrossRef]
93. United States Department of State. *U.S.-Caribbean Partnership to Address the Climate Crisis 2030*; U.S. Department of State: Washington, DC, USA, 2025. Available online: https://www.state.gov/pacc2030/ (accessed on 15 June 2025).
94. Ince, D.; Vredenburg, H.; Liu, X. Drivers and inhibitors of renewable energy: A qualitative and quantitative study of the Caribbean. *Energy Policy* **2016**, *98*, 700–712. [CrossRef]
95. Driver, T. Caribbean Energy 2024: Prospects, Challenges & Opportunities for Oil & Gas, Renewables and Environment. 2024. Available online: https://cpccaribbean.org/caribbean-energy-2024-prospects-challenges-opportunities-for-oil-gas-renewables-and-environment/ (accessed on 11 September 2026).
96. Gustafson, B. The New Energy Imperialism in the Caribbean: The Caribbean has some of the highest utility rates in the world. Decades of fossil fuel dependence, foreign profiteering, and domestic debt made it so. *Nacla Rep. Am.* **2017**, *49*, 421–428. [CrossRef]
97. Lu, S.; Gao, Z.; Zhang, P.; Xu, Q.; Xie, T.; Zhang, A. Event-triggered federated learning for fault diagnosis of offshore wind turbines with decentralized data. *IEEE Trans. Autom. Sci. Eng.* **2023**, *21*, 1271–1283. [CrossRef]
98. Jia, S.; Gao, Z.W. Benchmark model and dynamic analysis for floating offshore wind turbines. *Control Eng. Pract.* **2026**, *174*, 107062. [CrossRef]
99. Masson, M.; Ehrhardt, D.; Lizzio, V. Sustainable Energy Paths for the Caribbean. 2020. Available online: https://publications.iadb.org/en/sustainable-energy-paths-caribbean (accessed on 11 September 2026).
100. Michalena, E.; Hills, J. Renewable energy issues and implementation of European energy policy: The missing generation in Small Island Developing States. *Energy Policy* **2018**, *115*, 445–457. [CrossRef]
101. Lucas, H.; Fifita, S.; Talab, I.; Marschel, C.; Cabeza, L.F. Critical challenges and capacity building needs for renewable energy deployment in Pacific Small Island Developing States (Pacific SIDS). *Renew. Energy* **2017**, *107*, 42–52. [CrossRef]
102. Atkinson, T.; Preckel, P.V.; Gotham, D. Costs and trade-offs associated with renewable energy policies for Small Island Developing States: Case study for Jamaica. *Socio-Econ. Plan. Sci.* **2022**, *84*, 101374. [CrossRef]
103. Pratama, Y.W.; Gidden, M.J.; Greene, J.; Zaiser, A.; Nemet, G.; Riahi, K. Learning, economies of scale, and knowledge gap effects on power generation technology cost improvements. *iScience* **2025**, *28*, 111644. [CrossRef] [PubMed]
104. Powering the Blue Economy: Exploring Opportunities for Marine Renewable Energy in Maritime Markets. Available online: https://www.blueclimateinitiative.org/sites/default/files/2020-12/Powering%20the%20Blue%20Economy%20Report%2073355-v2-sm2.pdf (accessed on 11 September 2026).

105. Grand View Research. Tidal Energy Market Size, Share and Growth Report, 2030. 2025. Available online: https://www.grandviewresearch.com/industry-analysis/tidal-energy-market-report (accessed on 13 June 2025).
106. Thompson, B.S. Blue bonds for marine conservation and a sustainable ocean economy: Status, trends, and insights from green bonds. *Mar. Policy* **2022**, *144*, 105219. [CrossRef]